China Steel Technical Report, No. 36, pp.46－52, (2023)

A Study on the Oxidation Behavior of Self-Sintered Graphite Blocks

JEN-YUNG HSU*, YUNG-LIN YEN, WEI-CHENG WU** and TUNG-HSIN SU***

**New Material Research and Development Department*
***Research and Development Department*
China Steel Chemical Corporation

The oxidation behavior of self-sintered graphite blocks was studied using the thermogravimetric analysis method together with microstructure observation: a conventional pitch-impregnated graphite block was also investigated for comparison. To investigate the oxidation reaction kinetics, the samples were isothermally oxidized at 750ºC and 800ºC. As the oxidation temperature was high enough, the influence of the diffusion of oxygen molecules became insignificant, and the oxidation rate increased with decreasing particle size of raw materials, most likely due to the increase in the amount of the active site's free surface. All the reaction curves showed a sigmoidal shape and could be well described by a nucleation and growth model. The fitting results indicated that the conventional sample had a higher growth dimension, suggesting that once the reaction was triggered in the specimen, the oxidation could spread over the entire sample quickly. The oxidized artifact made of the conventional graphite block showed homogeneous oxidation morphology, while the growth of oxidation was limited in the self-sintered one. The resultant morphology is quite consistent with the kinetics study results.

Keywords: Graphite Blocks, Oxidation, Kinetics, Morphology

1. INTRODUCTION

Graphite blocks possess promising heat resistance and thus are widely used in elevated temperatures. For example, graphite electrodes, crucibles, and casting molds for metal are some common applications. For those graphite artifacts utilized under high-temperature conditions, their oxidation behavior crucially affects the material service life.

Several works[1-2] have been dedicated to understanding the mechanism of the oxidation of graphite materials. The kinetics of the graphite oxidation is quite complicated. Here is a brief overview, the oxidation process includes the adsorption of oxygen onto the graphite surface, oxidation reactions, and desorption of CO and CO_2 gasification products.

In the first stage of oxidation, oxygen atoms must adsorb onto the active free site of the graphite. The adsorption depends on the reactivity and validation of the free sites, the affinity of the oxygen atoms to the graphite surface, and the stability of the resulting complexes. The oxygen atoms can form ethers, lactones, and acid anhydrides embedded in the crystal basal planes. In addition, the formation of carbonyl complexes and alcohols is also possible typically occurring at the edges of basal planes[3]. Therefore, the amounts of the active site-free surface (ASA) would significantly affect the reactivity of graphite specimens, which are dominated by the crystalline structure and the fabrication method of the graphite blocks.

Before the adsorption of oxygen atoms, the oxygen molecules must diffuse through the bulk fluid phase toward the surface of the specimens. In some cases, the oxygen molecules could further diffuse into the materials via their pore structure. Therefore, the porosity and pore connectivity can also affect the oxidation behavior of graphite materials[1]. If the oxygen molecules can diffuse through internal pores, the oxidation reaction will occur inside the bulk graphite. Otherwise, the reaction only takes place at the surface of the materials.

To fabricate graphite blocks, raw carbonaceous powders are first molded, followed by heat treatments for carbonization and graphitization. A conventional process is commonly applied using cokes and pitch binders as raw materials and thus additional pitch impregnation procedure for densification is needed. However, the intrusion of pitches could damage the homogeneity of the graphite artifacts[4]. Another kind of graphite block was developed using binding carbon powder (BCP) as the raw materials[5] and due to the self-sintering function provided by BCP, no additional pitch impregnation treatment is needed. Those graphite

blocks made of BCP have been found to exhibit high mechanical strength, and their homogeneity of density and flexural strength is remarkable[6]. This type of product is usually called self-sintered graphite blocks to be distinguished from those made by the conventional process.

Since the oxidation process is complicated, it is quite difficult to evaluate the reaction rate of each stage separately. Instead, it is more practical to measure the overall oxidation rate. Several works[7-8] have used the thermogravimetric analysis (TGA) method to characterize the oxidation behavior. By examining the development of the reaction rate, it is possible to deduce the mode of the gasification process and to extract oxidation rate parameters that can be used for constructing predictive models. In the present work, the oxidation behaviors of self-sintered and conventional graphite blocks have been comparatively studied.

2. EXPERIMENTAL METHODS

2.1 Sample Preparation

The BCP was synthesized by the China Steel Chemical Corporation, Taiwan. The average particle size of the powder was controlled by pulverization and cyclone separation. Three categories of BCPs exhibiting distinct particle sizes have been used in the present study. Those BCPs with median particle size D50 of 20 μm, 12 μm, and 7 μm were synthesized and abbreviated as BCP-20, BCP-12, and BCP-07, respectively.

To fabricate graphite blocks, BCPs with different particle sizes were molded by cold isostatic pressing at the same pressure to form a green body with a dimension of Φ80 mm×H130 mm and a density of 1.28 - 1.32 g/cm^3 followed by carbonization and graphitization treatments.

2.2 Oxidation Kinetics

The oxidation kinetics of the graphite blocks were examined by the TGA system (STA7200, Hitachi). The samples were cut into small pieces with the dimensions of 2×2×2 mm^3. The specimens were quickly heated at a rate of 20ºC/min up to the desired temperatures (750 and 800ºC) in an N_2 atmosphere, followed by isothermal for 1 - 2 hrs in the air to conduct an oxidation reaction. The weight loss profiles during oxidation were then recorded for further analysis.

2.3 Field Tests and Morphology Observation

The graphite blocks made of BCP-12 were machined into electrode connectors, which are important components of the heating elements, to conduct heating current in a vacuum-melting furnace. Additional connectors made of a conventional graphite block (denoted as CG-T), which are a commercial product of T company in Japan and widely adopted in this application, were also used for comparison. The furnace was heated up to 1000 – 1100ºC followed by cooling back to room temperature in a vacuum every single run. Each set of heating elements was used for 30 runs and then dismantled. The oxidized connectors were sliced, cold-mounted in epoxy resin, and then examined with scanning electron microscopy (SEM; JSM-IT100, JEOL) to investigate the morphology of graphite after oxidation.

3. RESULTS AND DISCUSSION

3.1 Sample Characterization

The BCPs with different particle sizes were separately applied to fabricate graphite blocks, and those samples derived from BCP-20 were designated as SG-20 and so on. The degree of graphitization (DG) of graphite blocks was determined by an X-ray diffraction technique[9]. The values of DG and the physical properties of the self-sintered graphite blocks were measured as shown in Table 1. Those properties in Table 1 were measured for CG-T as well. The graphitization process was carefully controlled such that the values of DG of the self-sintered graphite blocks were similar. As for the physical properties, the density and hardness of the derived graphite block gradually increased with the decrease in BCP's particle size. Besides, the densities of the self-sintered graphite blocks were all higher than CG-T.

Table 1 Physical properties of the self-sintered and conventional graphite blocks

sample	DG (%)	Density (g/cm^3)	Hardness (Shore D)
SG-20	81	1.87	62
SG-12	81	1.90	64
SG-07	84	1.92	65
CG-T	78	1.77	51

3.2 Oxidation Kinetics Analysis Results

The graphite blocks were rapidly heated to 750 or 800ºC and then subjected to an isothermal oxidation process. Their weight loss during isothermal oxidation at the desired temperatures was recorded by the TGA instrument as depicted in Figure 1. The degree of reaction, α, defined as follows with m_0 being the starting mass and m the mass at oxidation time, t, was calculated according to the TGA data and shown in Figure 2.

$$\alpha(t) = \frac{m_0 - m(t)}{m_0} \quad \text{..... (1)}$$

The reaction rate of oxidation can be generally factorized as the following equation[10].

$$\frac{d\alpha}{dt} = k(T)f(\alpha)P_{O_2} \quad \text{..... (2)}$$

where k(T) is the reaction constant that depends on temperature, T, f(α) represents the conversion function that depends on the reaction model, and P_{O_2} the partial pressure of oxygen. Since the air gas stream continuously flowed through the sample holder of the TGA apparatus as the oxidation process was conducted isothermally, k(T) and P_{O_2} can be deemed as constant.

In the case where the specimens were oxidized at 750ºC, the self-sintered graphite blocks gasified more slowly than the conventional one, CG-T. It has been found[1] that while oxidation takes place at moderate temperatures, the diffusion of oxygen molecules into the specimens has a significant influence on the oxidation rate. Since all the self-sintered samples are denser than CG-T, they may suppress the diffusion of oxygen molecules and thus are more resistant to oxidation.

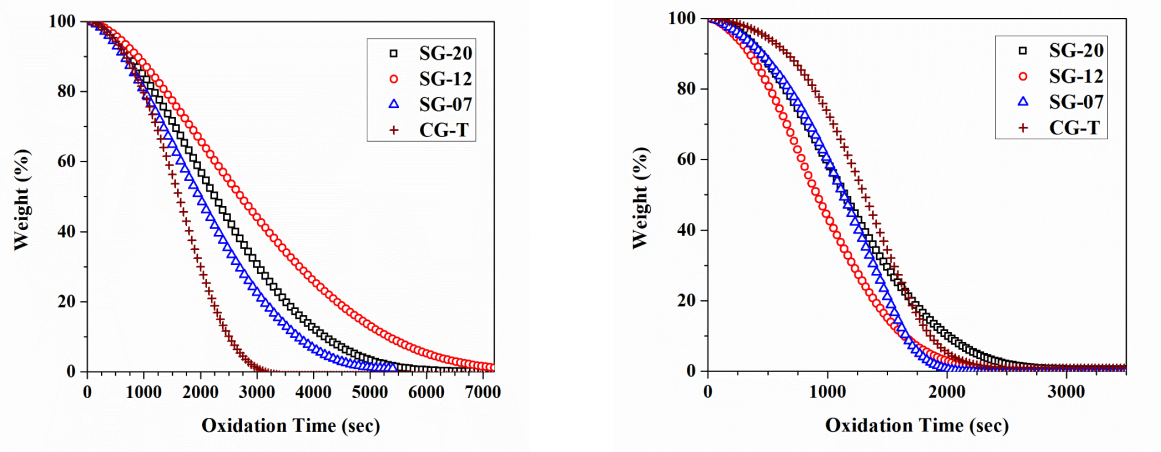

(a) (b)

Fig.1. Weight loss profiles for the isothermal oxidation of graphite blocks conducted at (a) 750°C and (b) 800°C.

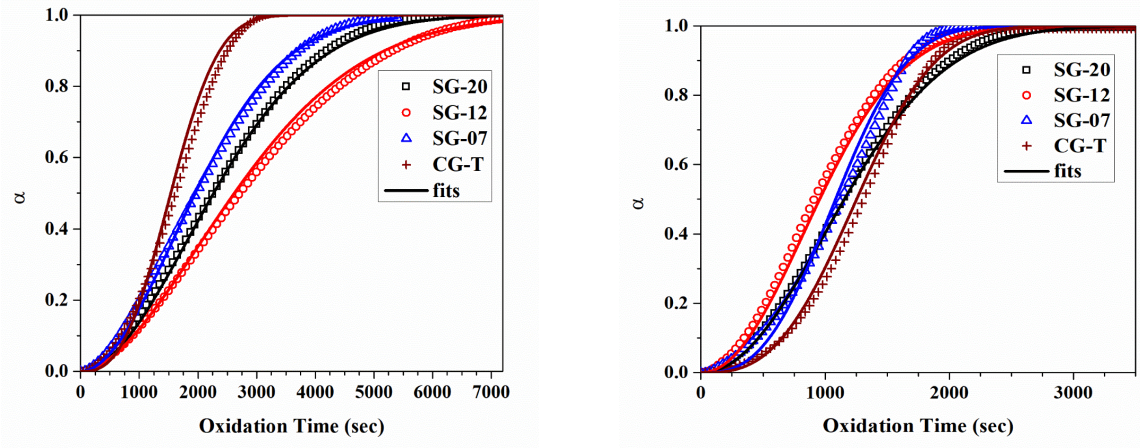

(a) (b)

Fig.2. Plots showing α vs t for the isothermal oxidation of graphite blocks conducted at (a) 750°C and (b) 800°C.

In addition, the oxidation rate of self-sintered graphite blocks with different particle sizes was compared. Figure 1a shows the sequence of the overall reaction rate of SG-12 < SG-20 < SG-07. The effects of the particle size of raw materials on the derived graphite blocks were complex. As the particle size decreased, its graphite block's density increased and the diffusion of oxygen molecules into the specimens was presumed to be limited, which might lead to a decrease in oxidization rate.

Nevertheless, the finer particles could also escalate the oxidization rate. Unlike conventional graphite, which has been repeatedly impregnated with pitches, the constituting particles of self-sintered graphite blocks are not covered with additional pitches. The constituting particles are inferred to be exposed to the atmosphere, and thus the graphite blocks with finer raw materials had higher oxidation rates owing to their high specific surface areas, which provides more amounts of ASA. The sequence of the reaction rate was thus dominated by the complex effects of oxygen diffusion and ASA content.

While oxidation took place at 800ºC, the oxidation rate for all the samples was enhanced significantly. According to Figure 1b, the reaction time to complete oxidation for SG-20 is slightly longer than SG-12, which is more than SG-07, indicating that the sequence of the overall reaction rate is SG-20 < SG-12 < SG-07. Since the influence of oxygen diffusion into specimens is insignificant at high temperatures, the oxidation rate is probably dominated by the amounts of ASA and thus the reaction rate is enhanced with the decrease of particle size.

The sigmoidal shape of the α vs t curves revealed in Figure 2 indicates that all the specimens studied in the present work are most likely oxidized through nucleation and growth mechanism[11]. The oxidation profiles can thus be fitted to the Johnson-Mehl-Avrami-Erofeyev-Kolmogorov (JMAEK) equation[12] displayed as follows.

$$f(\alpha) = n(1-\alpha)(-\ln(1-\alpha))^{\frac{n-1}{n}} \quad \text{.....(3)}$$

By applying the JMAEK equation, α can be estimated as follows.

$$\alpha = 1 - \exp(-(\mathrm{Kt})^{\mathrm{n}}) \quad \text{.....(4)}$$

where K is the effective rate constant, and n is the Avrami exponent depending on the growth dimension. The fitting curves are depicted in Figure 2 and the resultant parameters are listed in Table 2. For the self-sintered graphite blocks, in the cases where oxidation took place at 750ºC, the Avrami exponents of the samples were similar, namely 1.8-1.9, while their effective rate constants were different due to the complex effects of oxygen diffusion and ASA content. In the cases where oxidation took place at 800ºC, the oxidation rate was significantly enhanced. For SG-20 and SG-12, their Avrami exponents increased slightly to 2.1 while the effective constants increased notably. Since K is affected by the energy barrier of oxidation, the increase in K could be attributed to the prone to oxidation probably due to the increase in the amounts of ASA. As the size of BCP decreased from 12 μm to 7 μm, their K remained similar while their Avrami exponents dramatically increased from 2.1 to 2.8. Since n is affected by the growth dimensions during the oxidation process, the increase in n suggested that once the oxidation was initiated in SG-07, the oxidation reaction would consume the specimen more quickly.

For CG-T, its Avrami exponents were quite high, namely 2.8-2.9, no matter whether the oxidation took place at 750ºC or 800ºC. This indicated that the growth dimension of CG-T tended to be relatively high compared to the self-sintered samples, indicating that once the reaction was triggered in CG-T, the oxidation was more likely to spread over the entire sample.

3.3 Morphology Observation Results

The specimens of SG-12 and CG-T were polished and then subjected to SEM observation. The obtained

Table 2 Fitted parameters for the oxidation of graphite blocks.

sample	oxidation at 750 ℃		oxidation at 800 ℃	
	K (1/sec)	n	K (1/sec)	n
SG-20	3.6×10^{-4}	1.9	7.4×10^{-4}	2.1
SG-12	3.1×10^{-4}	1.8	8.8×10^{-4}	2.1
SG-07	4.2×10^{-4}	1.9	8.1×10^{-4}	2.8
CG-T	5.7×10^{-4}	2.8	7.0×10^{-4}	2.9

micrographs are shown in Figure 3. The microstructure of SG-12 exhibited constituting particles sintered by binding materials, which was a typical morphology of a self-sintered graphite block. For CG-T, the framework was embedded in flowable materials, suggesting that the sample has been repeatedly impregnated with pitches.

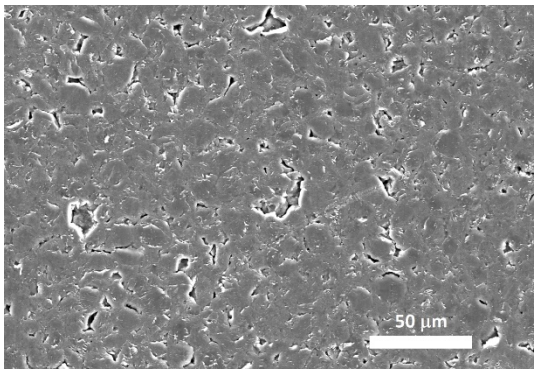

(a)

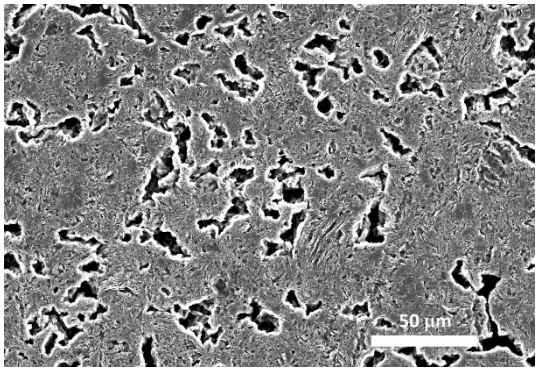

(b)

Fig.3. SEM micrographs of (a) SG-12 and (b) CG-T.

Both SG-12 and CG-T were made into electrode connectors and then subjected to field tests. After the tests, both samples were significantly corroded, thinning, and fragile as shown in Figure 4. For the oxidized CG-T, large flakes have peeled off the artifact, while for corroded SG-12, only the surface has prominently deteriorated and become chalky. The appearance of the used artifacts was quite different. The cross sections of both oxidized connectors were obtained and shown in Figure 5. For the SG-12 sample, there was a clear boundary between the region near the surface and the core. On the other hand, it was homogeneously oxidized for the CG-T sample and no boundary was observed. The appearance of their cross-sections showed significant differences. Both samples were thus cold-mounted such that the morphologies of the used artifacts were properly preserved, and SEM probation was conducted to investigate their microstructure.

(a) (b)

Fig.4. Oxidized connectors made of (a) SG-12 and (b) CG-T.

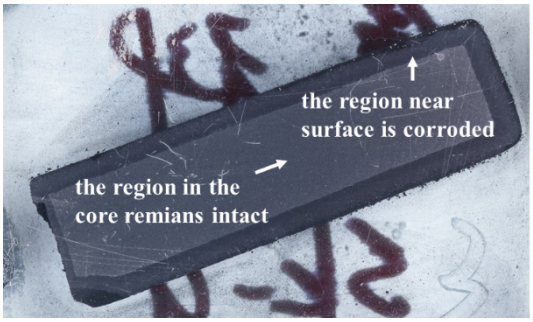

(a)

(b)

Fig.5. Cross sections of the oxidized connectors made of (a) SG-12 and (b) CG-T.

The SEM micrographs of the cross-section of oxidized SG-12 are illustrated in Figure 6. The materials near the surface have been severely corroded while those near the core remained intact. Interestingly, there was a clear boundary between those two areas as indicated by a dashed line in Figure 6. This suggested that the oxidation reaction gradually declined away from the surface of the artifact. However, for the oxidized

CG-T, there were no areas that remained intact as displayed in Figure 7, suggesting that the specimen was homogeneously oxidized. The TGA analysis showed that during the oxidation process, the occurrence of the reaction could easily spread over the entire sample in the CG-T case. On the other hand, the spread of oxidation in SG-12 was limited. The oxidation behavior of the comparative specimens in the field tests was quite consistent with the TGA analysis results.

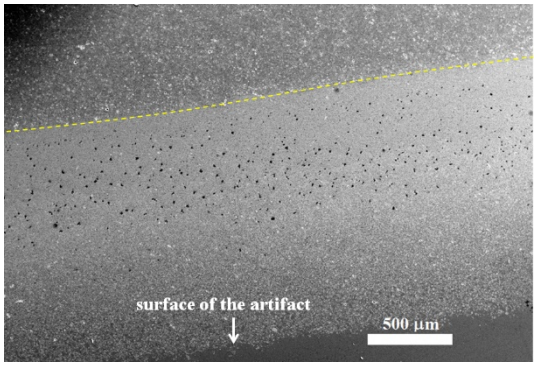

(a)

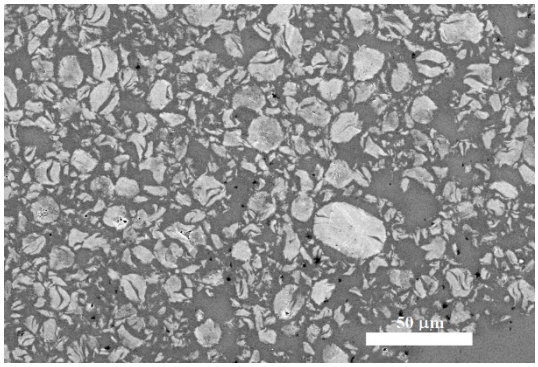

(b)

Fig.6. (a) SEM micrographs of the oxidized artifact made of SG-12 and the subplot (b) showing the enlargement of the region near the surface. There is a boundary indicated by a dashed line.

For those corroded areas as shown in Figure 7, only large particles were sustained while small particles were gasified. This phenomenon was also observed in the corroded SG-12 sample as shown in Figure 6b. By comparing the morphology of the region near the surface and that near the core, it could be found that small particles have vanished in the corroded region. This indicated that the oxidation process for CG-T and SG-12 had some common features that small constituting particles were more prone to gasification than large ones. This is also consistent with the TGA results as mentioned in the previous discussion.

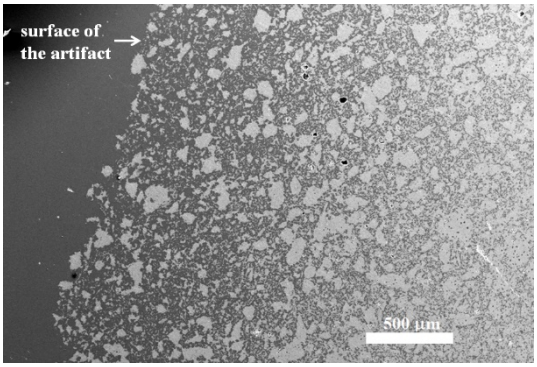

(a)

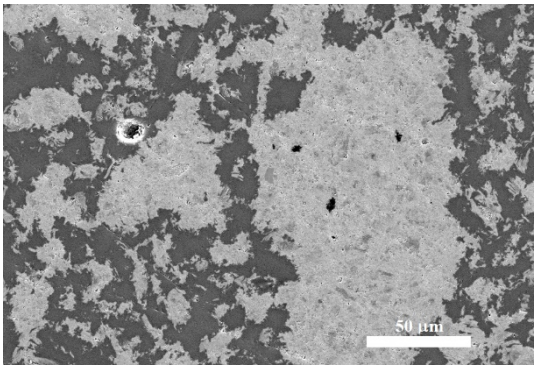

(b)

Fig.7. (a) SEM micrographs of the oxidized artifact made of CG-T and the subplot (b) showing the enlargement of the region near the surface.

4. CONCLUSIONS

The oxidation behavior of the self-sintered and conventional graphite blocks was investigated by TGA analysis and morphology observation. All of the samples exhibited sigmoidal α vs t curves during isothermal oxidation experiments, which could be described by the JMAEK equation. According to the analysis results, CG-T tended to have a higher Avrami exponent compared to the self-sintered materials, indicating CG-T had a higher growth dimension during the oxidation process. SG-12 and CG-T were further subjected to field tests and underwent repeated heating and cooling in a vacuum furnace. After the tests, the spread of oxidation in the SG-12 sample was limited with its cord region remaining intact. However, the CG-T sample showed homogeneous oxidation morphology over the entire sample, which is quite consistent with the TGA results.

REFERENCES

1. M. S. El-Genk and J. M. P. Tournier, Development and validation of a model for the chemical kinetics of graphite oxidation, J. Nucl. Mater., 2011, vol. 411, pp. 193-207.
2. K. Leistner, A. Nicolle, D. Berthout and P. da Costa,

Kinetic modelling of the oxidation of a wide range of carbon materials, Combust. Flame, 2012, vol. 159, pp. 64-76.
3. B. Marchon, J. J. Carrazza, H. Heinemann and G. A. Somorjai, TPD and XPS studies of O_2, CO_2, and H_2O adsorption on clean polycrystalline graphite, Carbon, 1988, vol. 26, pp. 507-514.
4. T. Arai, S. Sato, and T. Oku, Assessment of heterogeneity and anisotropy of IG-110 graphite for nuclear components, J. Nucl. Sci. Technol., 1991, vol. 28, pp. 713-720.
5. J. Y. Hsu, C. J. Su, Y. L. Yen, and C. Y. Lee, Effects of chemical composition of carbonaceous powder on the morphology and thermal properties of graphite blocks, Carbon Lett., 2022, vol. 32, pp. 797-805.
6. K. Shen, Z. H. Huang, W. Shen, J. Yang, G. Yang, S. Yu and F Kang, Homogenous and highly isotropic graphite produced from mesocarbon microbeads, Carbon, 2015, vol. 94, pp. 18-26.
7. C. I. Contescu, S. Azad, D. Miller, M. J. Lance, F. S. Baker and T. D. Burchell, Practical aspects for characterizing air oxidation of graphite, J. Nucl. Mater., 2008, vol. 381, pp. 15-24.
8. A. K. Singh, X. M. Hou and K. C. Chou, The oxidation kinetics of multi-walled carbon nanotubes, Corros. Sci., 2010, vol. 52, pp. 1771-1776.
9. N. Iwashita, C. R. Park, H. Fujimoto, M. Shiraishi and M. Inagaki, Specification for a standard procedure of X-ray diffraction measurements on carbon materials, Carbon, 2004, vol. 42, pp. 701-714.
10. S. Vyazovkin and C. A. Wight, Isothermal and non-isothermal kinetics of thermally stimulated reactions of solids, Int. Rev. Phys. Chem., 1998, vol. 17, pp. 407-433.
11. A. Khawam and D. R. Flanagan, Solid-state kinetic models: basics and mathematical fundamentals, J. Phys. Chem. B, 2006, vol. 110, pp. 17315-17328.
12. W. A. Johnson and R. F. Mehl, Reaction kinetics in processes of nucleation and growth, Trans. AIME, 1939, vol.135, pp. 416-442.